CFSRC COLLOQUIUM

Proceedings of the Cold-Formed Steel Research Consortium Colloquium
20-22 October 2020 (cfsrc.org)

Study on Sectional-Global Interaction Buckling of Stainless Steel Lipped-C Beam-Columns

Yueming Yang[1], Kang Han[2], Shuang Niu[3]

Abstract

As part of a research series concerning sectional and member capacity of cold-formed stainless steel beam-columns, this paper presents some experimental and simulated results on the interaction buckling behavior of stainless steel lipped-C beam-columns. Two series of tests (12 specimens in each series) were carried out first, for which the cross-section geometry and end restraints of specimens were designed to obtain distortional-global and local-global interaction buckling respectively. The experiments involved two alloys (austenitic S30401 (1.4301) and duplex S32205 (1.4462)) and three loading eccentricity levels (none, small and large). A detailed finite element model based on ABAQUS was developed and verified against test date.

1. Introduction

Stainless steel has excellent corrosion resistance and durability, good fire resistance, and good low temperature toughness. The good ductility and plasticity of stainless steel make it easy to process into thin-walled components.[1-3] At present, there are more and more applications of stainless steel materials in the field of building structures, and various countries have also issued stainless steel specifications and technical regulations.[4-6] Stainless steel structures will have more and more extensive applications and developments in the future.

Different from ordinary carbon steel, stainless steel has no obvious yield point and yield platform. People are used to taking the stress corresponding to the 0.2% residual deformation of stainless steel as the nominal yield stress of the material. This feature is manifested in the structural behavior that the critical instability load will decrease and the deformation will increase. The stress strengthening effect may contribute to the bearing capacity of the component in some cases.

The study on stainless steel compression members and bending members has been in-depth and extensive. In recent years, many experts and scholars focus on the study of stainless steel bending components. Yuner Huang and Ben Young[7] conducted a test program on cold-formed lean duplex stainless steel SHS and RHS members in combined compression and minor axis bending. Ou zhao and Leroy[8-10] Gardner conducted ferritic stainless steel tubular beam-column members subjected to unequal end moments. Still, they made efforts on study of cold-formed stainless steel CHS beam-columns. Baofeng Zheng[11] conducted tests of cold-formed and welded stainless steel beam-columns. Keyang Ning and Lu Yang[12] studied the flexural buckling behavior and design of wielded stainless steel box-section beam-columns. Merih Kucukler and Leroy Gardner[13] conducted tests of flexural-torsional buckling of austenitic stainless steel I-section beam-columns and other related numerical modeling and design. This paper presents an experimental study on the cold-formed stainless steel lipped-C beam-columns and a research project of calibrating FE models.

2. Materials

Test coupons were processed from 2440mm x 1220mm x 1.84mm austenitic S30401 and duplex S32205 stainless steel virgin flat sheets (Alloy name following the ASTM unified numbering system). In order to truly reflect the mechanical properties of cold-formed thin-walled stainless steel materials, considering the anisotropy of the material, the specimens were cut along the longitudinal, diagonal and transverse directions in the stainless steel virgin flat sheets.

Table 1

Stainless steel material mechanical properties

	f0.01/ MPa	f0.2/ MPa	fu/ MPa	E0/ MPa	n	εt/%
304L	155	245	772	198672	6.54	59.9
304D	166	249	778	201190	7.38	60.48
304T	150	256	810	203117	5.60	60.42
2205L	316	551	784	202756	5.38	41.92

[1] Graduate Research Assistant, School of Civil Engineering, Harbin Institute of Technology, tumuyym@126.com
[2] Graduate Research Assistant, School of Civil Engineering, Harbin Institute of Technology, kanghan3705@outlook.com
[3] Assistant Professor, School of Civil Engineering, Harbin Institute of Technology,.aniu216@126.com

2205D	330	575	785	201795	5.39	40.67
2205T	361	588	825	191788	6.14	38.75
304Cor	275	558	860	206641	4.23	32.12
2205Cor	388	768	998	205036	4.38	12.1

(a) L, D and T represent longitudinal, diagonal and transverse direction. The 'cor' represents the cold-formed corner part of lipped-C section.

3. Design of Member

Stainless steel beam-columns tested in this paper were all lipped-C section. This paper's experiment would like to focus on the sectional-global interaction buckling of stainless steel lipped-C beam-columns. Therefore, 2 different sectional buckling (distortional buckling and local buckling) must be included in the tests. The first section of the test should satisfy that distortion buckling occurred before local buckling. The second section of the test should satisfy that local buckling occurred before distortion buckling. The test section design was conducted with software CUFSM. By using CUFSM, it was convenient and accurate to obtain the relationship curve between the half-wave length of elastic buckling and corresponding critical load, and then the critical stress of distortional buckling and local buckling could be determined. The dimension of lipped-C cross-section is presented in Fig 1, H, B, a, t, r represent the cross-section height, flange width, lip height, thickness and corner external radius. In order to study the sectional-global interaction buckling, the member length was determined to be 1500mm. The geometry of section A and B is shown in table 6. For section A, the interaction between distortional buckling and torsional-flexural buckling would be studied. For section B, the interaction between local buckling and flexural buckling would be studied.

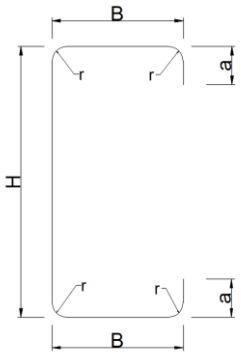

Fig.1 Nomenclature for C section dimensions

Table 2

Section geometry

Section	H/mm	B/mm	a/mm	t/mm	r/mm	Length/mm
Section A	120	80	10	1.85	4	1500
Section B	150	60	20	1.85	4	1500

In order to study the influence of different eccentricity on the sectional-global interaction buckling, three loading conditions were designed, namely axial compression, small eccentric compression and large eccentric compression shown in Fig.2, and the eccentricity was calculated according to the bending moment distribution. The σ 1 represented the minimum section stress, while σ 2 represented the maximum section stress. When the member was under axial pressure, σ 1/ σ 2=1. When the member was under small eccentric pressure, σ 1/ σ 2=0.5. When the member was under large eccentric pressure, σ 1/ σ 2=0. The member of section A was designed for distortional buckling and global buckling around the strong axis (e_α =0, e_β =-14mm, e_γ =-42mm). The member of section B was designed for local buckling and global buckling around the weak axis (e_α =0, e_β =-5.4mm, e_γ =-12.9mm).

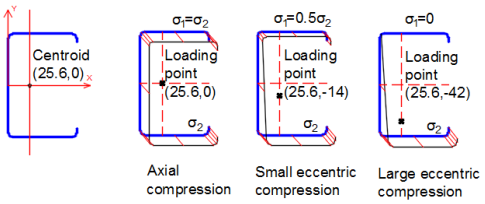

(a) Section A loading eccentricity

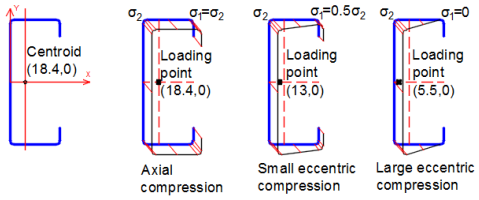

(b) Section B loading eccentricity

Fig.2 Bending moment distribution

The member would be named as “Material-Section type-Member length-Loading condition-Number”. Number means the first and second batch coupon tests respectively. For example, 2205BL β -1 means that the member was made of 2205 stainless steel, the section was B, the long column (not stub, distinguished from the stub test which was conducted by us), the small eccentric loading (α represented axial pressure, β represented small eccentric pressure, γ represented large eccentric pressure) and the number was 1.

4. Measurement of geometric imperfection

4.1 Measurement device

Cold-formed thin-walled stainless steel members are very sensitive to geometric imperfections. Therefore, it is necessary to make efforts to measure the geometric imperfections of cold-formed thin-walled stainless steel members. With a high-precision imperfection measurement device shown in Fig.7, the imperfection information of each member was convenient to obtain.

The equipment relied on the outer frame to set up two parallel linear aluminum alloy guide rails in the same horizontal plane, and a movable platform was set up in the middle of the guide rails shown in Fig.3 (a) and (b). The laser displacement meter could be fixed at any position through the groove on the platform to meet the measurement requirements of components of different sizes shown in Fig.3 (c). When working, the component to be measured was placed horizontally under the track and the platform, and the platform moved above the member to be measured at a uniform speed by a stepping motor. The laser displacement meter fixed on the platform continuously collected information of the distance from the surface of the member to the platform. Because the platform and the track were in the horizontal plane, the line representing the geometric information of the component surface could be obtained.

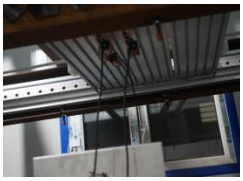

(a)Outer frame and guide rails

(b)Movable platform

(c)Grooves and laser displacement meter

(d)Measuring the geometric line of the member

Fig.3 Imperfection measurement device

4.2 Member measurement scheme

For the lipped-C section, the measurement points of cross section are shown in Fig.4. We could obtain 9 geometric data lines through measurement, which were used to describe the true geometric conditions of the member. The sampling frequency of the laser displacement meter was set to 55.86 Hz, which could ensure that enough geometric point data was obtained.

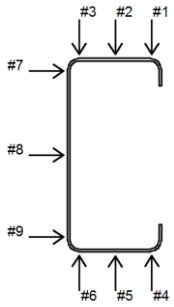

(a) Measurement points of cross section

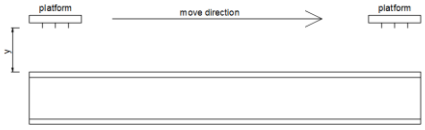

(b) Measurement platform direction

Fig.4 Imperfection measurement

4.3 Measurement result processing

Taking the measured imperfection data at line #1 of 304-ALα-1 member as an example, the imperfection curve is presented in Fig.5. The abscissa indicated the number of data points read by the laser displacement meter. The test member was 1500mm long, and each imperfection data line had about 810 data points. The ordinate represented the distance from the laser displacement meter to the surface of the member (the distance from the laser displacement meter to the surface of the member

was subtracted so that the readings at both ends were equal to 0). In order to accurately and conveniently represent the imperfection curve, a Fourier series is used to fit discrete imperfection points. And all the imperfection Fourier curves would be used for other analytical study.

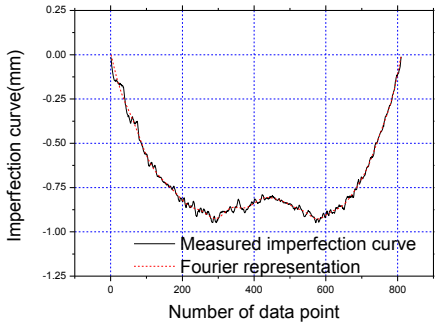

Fig.5 #1 measurement line imperfection curve of 304-ALα-1 member

5. Beam-columns test

5.1 Test set-up

This paper intended to explore the sectional-global interaction buckling of stainless steel beam-columns. In order to make the actual loading process of the test accord with the test design, a test loading set-up with unidirectional hinged ends was designed shown in fig.6. The bearings were used to achieve the purpose of one-way articulation and each bearing was bolted to the supporting part through the clamping part. The trapezoidal steel plate had 2 long holes. During loading, the trapezoidal steel plates and the member end plate closely fit due to the axial pressure shown in fig.7. The trapezoidal steel plates and the member end plate were connected by bolts. But during the loading process, the safety bolts were not subjected to force and played a protective role. High-strength plaster was used at the end of the member to fix the component curling and prevent it from warping. The calculated length of the member was the distance between the two rotation centers (that was the centers of the upper and lower steel bars).

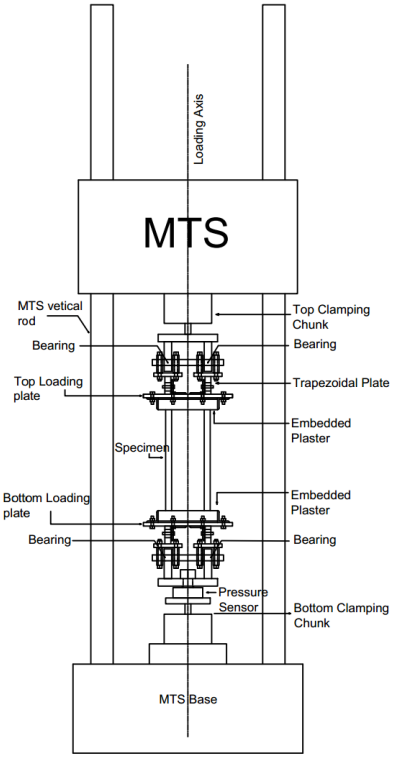

(a) Front elevation of test-up

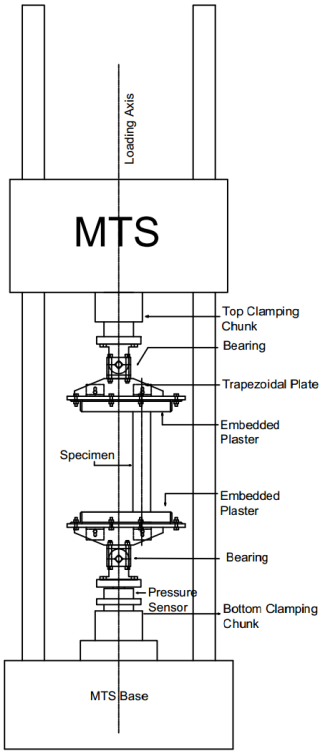

(b) Side elevation of test set-up

Fig.6 Test set-up

Fig.7 Bearing and trapezoidal plate

By this set of test equipment, we could carry out compression and bending tests on specimens of any section (the size of the specimen section should be smaller than the size of the end plate and the eccentricity should be smaller than the size of the end plate).

5.2 Loading scheme

The specimen was loaded on a 2500kgMTS electro-hydraulic servo testing machine. The loading rate was 0.1mm/min. When the load reaches 80% of the estimated ultimate bearing capacity of the member, the rate was adjusted to 0.05mm/min. In this way, the plasticity of the member could be developed. For section B members where local buckling occurred, the loading was continued after 3 minutes after loading to the ultimate load. Distortional buckling occurred for the section A members, and the bearing capacity of distortional buckling members dropped quickly, so the loading would not suspend.

5.3 Test phenomenon

A total of 24 beam-column compression and bending tests were carried out, including 12 section A specimens and 12 section B specimens. In section A specimens tests, distortion buckling and global flexure-torsional buckling would be studied. For section B specimens, local buckling and global flexural buckling would be studied. The specimens all reached the expected buckling phenomenon.

For the test phenomenon of section A specimens shown in fig.8 (a), taking 304-ALα-2 as an example: the loading condition of this specimen was axial compression, and the ultimate bearing capacity was 71.39kN. When the vertical pressure at both ends of the specimen was 65kN, the flange began to deform shown in fig.8 (b). When the vertical pressure at both ends of the component reaches 71kN, the distortional buckling had been fully developed, and the deformed section bent and twisted shown in fig.8 (c) and (d). Then the vertical pressure at both ends began to decrease. 71kN was the ultimate bearing capacity of the specimen.

The ultimate bearing capacity of A-section compression-bending members decreased with the increase of eccentricity.

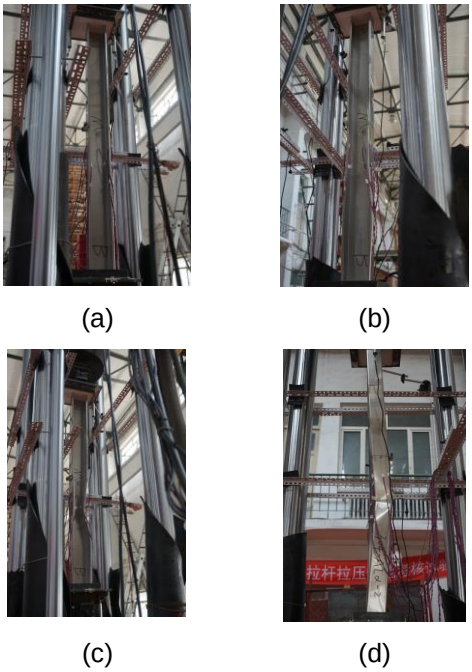

(a) (b)

(c) (d)

Fig.8 Loading process of specimen 304-ALα-2

For the test phenomenon of section B specimens, taking 2205-BLα-2 as an example: the loading condition of this specimen was axial compression shown in fig.16 (a), and the ultimate bearing capacity was 91.98kN. When the vertical pressure at both ends of the specimen was 80kN, the web began to bulge shown in fig .16 (b). When the vertical pressure at both ends of the component reaches 90kN, the global buckling began to develop. The specimen began to bend and the vertical pressure at both ends began to decrease at the same time shown in fig.9 (c) and (d).

The ultimate bearing capacity of B-section compression-bending members decreased with the increase of eccentricity.

(a) (b)

(c) (d)

Fig.9 Loading process of specimen 2205-BLα-2

6. FE models and verification

The FE models of cold-formed stainless steel lipped-C members under combined axial compression and uniaxial bending were established and calibrated through finite element analysis software ABAQUS in this subsection.

6.1 FE model settings

Element type: the S4R shell element

Member dimensions: the measured actual results of the member dimensions

Meshing: almost 4mm×4mm square grid for plate and 2mm×4mm rectangle grid for corner

Boundary conditions: Two reference points using rigid body constraint

6.2 Materials of FE models

The material properties of the flat area and the corner area were different, and different material properties should be given according to the results of the material property experiment. The true stress-strain curve of the material property experiment is input into the FE model.

6.3 Imperfection

We input the geometric imperfection of the test members actually measured into the FE model. Taking 2205-ALα-1 as an example, the geometric imperfection of this member is shown in Fig.10. In order to easily distinguish, the geometric imperfection in the figure has been enlarged 50 times.

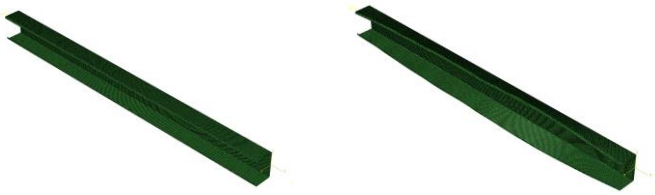

Fig.10 Members with imperfection

6.4 Verification

The key results of the test and the FE models, such as buckling modes of the members, bearing capacity, force-displacement curves, were summarized and compared.

6.4.1 Bearing capacity

As indicated in table 3, several ultimate bearing capacity of each FE model N_{FE} showed a good agreement with its corresponding test result N_u.

Table 3

Bearing capacity of members in test and FE models

Members	N_u/kN	N_{FE}/kN	N_u/N_{FE}
304ALα1	79.54	82.24	0.97
304ALα2	70.15	71.4	0.98
304ALβ1	65.13	64.46	1.01
304ALβ2	62.32	58.36	1.07
304ALγ1	44.278	46.5	0.95
304ALγ2	44.354	45.6	0.97
2205ALα1	110	112.3	0.98
2205ALα2	99.88	103.1	0.97
2205ALβ1	91.2	94.4	0.97
2205ALβ2	90.89	90.27	1.01
2205ALγ1	62.66	63.73	0.98
2205ALγ2	62.4	60.3	1.03

6.4.2 Buckling deformation

After comparing the buckling mode and overall deformation of all FE members with the actual test members, it could be seen from the example in fig.11 that they were relatively consistent.

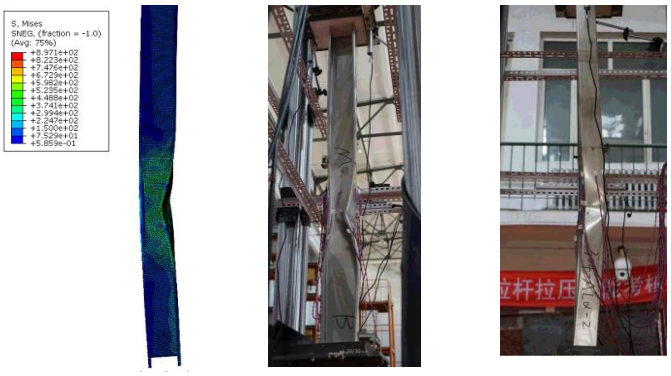

Fig.11 Buckling deformation

6.4.3 Force-displacement curves

We also compared the force-displacement curves of FE models with these of the tests. The parts of results were shown in fig.12.

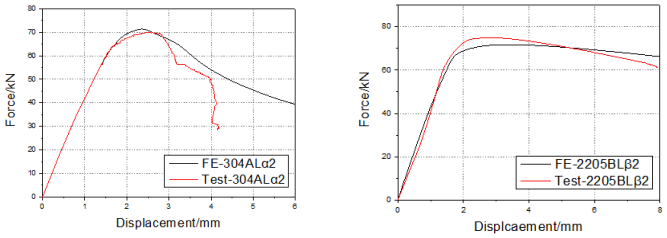

(a) 304Alα2 (b) 2205BLβ2

Fig.12 Comparisons of force-displacement curves

7. Conclusion

This paper introduces a series of tests on C-section austenitic 304 and duplex 2205 stainless steel beam-columns. This experiment mainly focused on three influencing factors: material, section buckling type, and eccentricity of load, to study the effect of interaction of sectional buckling and global buckling of stainless steel beam-columns on bearing capacity. The cross-section was designed to make the section A specimen develop distortional buckling and global flexural-torsional buckling and the section B specimens develop local buckling and global flexural buckling. The material properties and geometric imperfection of the specimens were measured before the test. Austenitic 304 and duplex 2205 have a certain degree of anisotropy, and cold-formed process has an impact on material properties.

A loading device was designed to ensure one-way hinged joints at both ends of the specimen. The position of the specimen could be adjusted to apply different eccentric load. All the tests achieved the expected interaction effect of sectional buckling and global buckling.

The FE model was established by using software Abaqus and compared with the test results. Comparing the three aspects of bearing capacity, buckling deformation, and force-displacement curves, the FE model could be in good agreement with the actual test results. It shows that the FE model is relatively close to the actual experimental situation, so it is reliable to use this model for subsequent parameter analysis.

References

[1] Lo K H , Shek C H , Lai J K L . Recent developments in stainless steels[J]. Materials science and engineering, 2009.

[2] Gardner L . The use of stainless steel in structures[J]. Progress in Structural Engineering and Materials, 2010, 7(2):45-55.

[3] Baddoo N R . Stainless steel in construction: A review of research, applications, challenges and opportunities[J]. Journal of Constructional Steel Research, 2008, 64(11):1199-1206.

[4] Australian/New Zealand Standard (AS/NZS 4673): cold-formed stainless steel structures. Sydney, Australia: Standards Australia/Standards New Zealand; 2001.

[5] Specification for the design of cold-formed stainless steel structural members (SEI/ASCE 8). American Society of Civil Engineers (ASCE). Reston, VA (USA): American Society of Civil Engineers (ASCE); 2002.

[6] Technical specification for stainless steel structures (CECS 410:2015). China Planning Press; 2015.

[7] Huang Y , Young B . Experimental investigation of cold-formed lean duplex stainless steel beam-columns[J]. Thin Walled Structures, 2014, 76(3):105-117.

[8] Buchanan C , Zhao O , Real Saladrigas E , et al. Cold-formed stainless steel CHS beam-columns: testing, simulation and design[J]. Engineering Structures, 2020, 213:110270.

[9] Zhao O , Gardner L , Young B . Experimental Study of Ferritic Stainless Steel Tubular Beam-Column Members Subjected to Unequal End Moments[J]. Journal of Structural Engineering, 2016, 142(11):04016091.

[10] Zhao O , Gardner L , Young B . Testing and numerical modelling of austenitic stainless steel CHS beam–columns[J]. Engineering Structures, 2016, 111(Mar.15):263-274.

[11] Baofeng, Zheng, Xia. Tests of cold-formed and welded stainless steel beam-columns[J]. Journal of Constructional Steel Research, 2015.

[12] Ning K , Yang L , Yuan H , et al. Flexural buckling behaviour and design of welded stainless steel box-section beam-columns[J]. Journal of Constructional Steel Research, 2019, 161(Oct.):47-56.

[13] Kucukler, M., L. Gardner and Y. Bu, Flexural-torsional buckling of austenitic stainless steel I-section beam-columns: Testing, numerical modelling and design. Thin-Walled Structures, 2020. 152.